Accepted Manuscript

Understanding difficulties of irregular number-membered ring transition states for intramolecular proton transfer in excited state

Xiaozhuan Qin, Ge Ding, Zhenqiang Wang, Yulong Gong, Fang Gao, Shengtao Zhang, Ziping Luo, Hongru Li

PII: S0040-4020(16)31304-7

DOI: 10.1016/j.tet.2016.12.026

Reference: TET 28318

To appear in: *Tetrahedron*

Received Date: 9 September 2016

Revised Date: 12 November 2016

Accepted Date: 13 December 2016

Please cite this article as: Qin X, Ding G, Wang Z, Gong Y, Gao F, Zhang S, Luo Z, Li H, Understanding difficulties of irregular number-membered ring transition states for intramolecular proton transfer in excited state, *Tetrahedron* (2017), doi: 10.1016/j.tet.2016.12.026.

This is a PDF file of an unedited manuscript that has been accepted for publication. As a service to our customers we are providing this early version of the manuscript. The manuscript will undergo copyediting, typesetting, and review of the resulting proof before it is published in its final form. Please note that during the production process errors may be discovered which could affect the content, and all legal disclaimers that apply to the journal pertain.

ACCEPTED MANUSCRIPT

Graphic Abstract

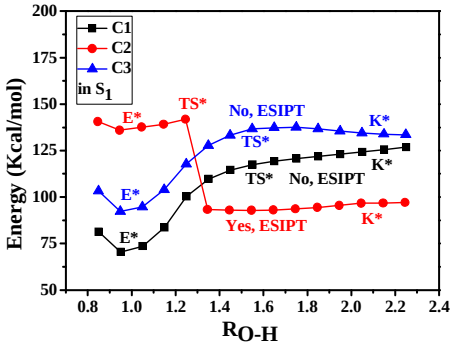

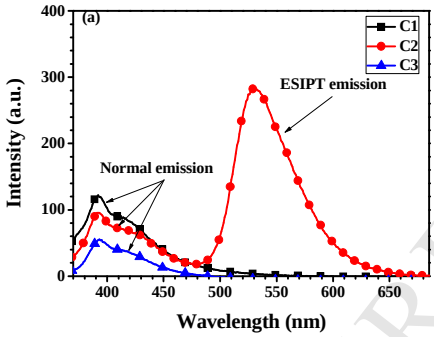

ACCEPTED MANUSCRIPT

ACCEPTED MANUSCRIPT

Understanding difficulties of irregular number-membered ring transition states for intramolecular proton transfer in excited state

Xiaozhuan Qin[1], Ge Ding[1], Zhenqiang Wang[1], Yulong Gong[1], Fang Gao[1, 2*], Shengtao Zhang[1, 2*], Ziping Luo[1, 2*], Hongru Li[1, 2*]

[1]College of Chemistry and Chemical Engineering, Chongqing University, Chongqing, China, 400044

[2]National-municipal Joint Engineering Laboratory for Chemical Process Intensification and Reaction, Chongqing University, Chongqing, China, 400044

Tel/Fax, 86-23-65102531, Emails, fanggao1971@gmail.com, stzhang@cqu.edu.cn, zpluo@126.com, hrli@cqu.edu.cn

ABSTRACT

This study presents a variety of organic dyes with similar molecular structures that could undergo intramolecular proton transfer in excited states via five-, six- and seven- number-membered ring transition states respectively. In addition, the dyes without proton transfer segments are also synthesized to use as references. X-ray single crystal diffraction, NMR spectra as well as UV/visible spectra suggests the presence of internal hydrogen bond with different strength in the target dyes. The steady and transient fluorescence measurements demonstrate occurrence of excited state intramolecular proton transfer via a six number-membered ring transition state. In contrast, it cannot be processed through five- and seven- number-membered ring transition states of the studied dyes. The molecular geometry optimization of the studied dyes reveals fundamental factors for the difficulties of intramolecular proton transfer in excited states via five- and seven- number-membered ring transition states.

Keywords: Proton transfer; Excited state; Transition sate; Organic dye; Molecular geometry optimization

1. Introduction

As one of the significant phenomena in life and nature, excited state intramolecular proton transfer (ESIPT) receives considerable experimental and theoretical interests.[1-6] The four-level cycle of enol and keto phototautomerization (E→E*→K*→K→E, E, enol, K, keto) is accepted as

the most representative mechanism to achieve ultrafast (femtosecond or sub-femtosecond time course) internal proton transfer in excited state of an organic molecule.[7-11]

Thus to an enol-keto ESIPT organic dye, there are two real chemical reactions in phototautomerization process, namely E^*-K^* and K-E. Accordingly, potential energy barrier of transition state for E^*-K^* phototautomerization of an organic dye plays crucial roles in occurrence of ESIPT. This suggests that formation and stability of transition state are significant to achieve an internal proton transfer in excited state of an organic dye.[12] Based on fundamental viewpoint, a tuned and well-defined barrier is of great importance for occurrence of enol-keto phototautomerization reaction of an organic chromophore.

Formation and stability of transition state of enol-keto phototatumerization of an organic dye is association with neighboring hydroxy and carbonyl or imino groups. Hence, transition state of enol-keto phototatumerization could be determined by intramolecular hydrogen bond strength, which is related to coplanarity as well as distance between proton donor and acceptor segments.

Owing to good stability, energy barriers of quasi six number-membered ring transition states yielded by adjacent hydroxy and imino or carbonyl groups in organic dyes are normally small or even barrierless. Hence, a number of organic dyes can undergo internal proton transfer in excited states via quasi six number-membered ring transition states.[13,14]

In view of the chemistry, a five number-membered ring structure possesses a similar stability as a six number-membered ring one. However, it is confused that only a few organic dyes were demonstrated to undergo intramolecular proton transfer in excited states via quasi five number-membered ring transition states.[15,16] It is considered that weak internal hydrogen bond can increase energy barriers of quasi five number-membered ring transition state of enol-keto

phototautomerization.

It is further observed that fewer organic dyes undergo intramolecular proton transfer in excited states via quasi seven number-membered ring transition states generated by neighboring proton donor and acceptor groups in organic dyes.[17-19] It is thought that energy barriers of enol-keto phototautomerization of organic dyes via quasi seven number-membered ring transition states can be increased by weak internal hydrogen bond.

Hence, enol-keto dye molecules may undergo ESIPT through six-membered ring transition states. In contrast, ESIPT occurs rarely via five- or seven- number-membered ring transition states of organic dyes. While so far, no studies have been carried out to reveal the difficulties of five- and seven- number-membered ring transition states for intramolecular proton transfer in excited states of organic dyes.

In this work, we present a series of organic dyes carrying proton donor and acceptor segments with similar molecular skeletons, which could undergo intramolecular proton transfer in excited states via different number-membered ring transition states. Meanwhile, the dyes lack of proton donor and acceptor groups are prepared to use as references. To the best of our knowledge, this is the first attempt to perform comprehensive experimental and theoretical studies to understand the difficulties of irregular number-membered ring transition states for intramolecular proton transfer in excited states of organic dyes.

2. Results and discussion

2.1. Internal hydrogen bond strength analyzed by X-single crystal diffraction analysis

Good single crystals of the target dyes were obtained through slow volatilization. **Figure 1** shows the presence of intramolecular hydrogen bond between the adjacent phenolic hydroxy and

imino groups in **C1**, **C2** and **C3** respectively. Internal hydrogen bond of these molecules was compared through analysis of dihedral angles and distances between hydroxy and imino groups based on X-single crystal diffraction.

Figure 1 suggests that **C1** and **C3** possess the longer H1-N1 (2.156 Å for **C1**, 1.844 Å for **C2**, 1.886 Å for **C3**) and N1-O1 (2.637 Å for **C1**, 2.572 Å for **C2**, 2.652 Å for **C3**) as well as the larger dihedral angles of ∠C-O1-H1-N1 (∠C2-O1-H1-N1 for **C1**, 2.96˚; ∠C3-O1-H1-N1 for **C2**, 0.62˚; ∠C8-O1-H1-N1 for **C3**, 10.71˚) in phenolic hydroxy and imino groups than **C2**. This indicates that there is a stronger internal hydrogen bond in **C2** comparing to that in **C1** and **C3** respectively.

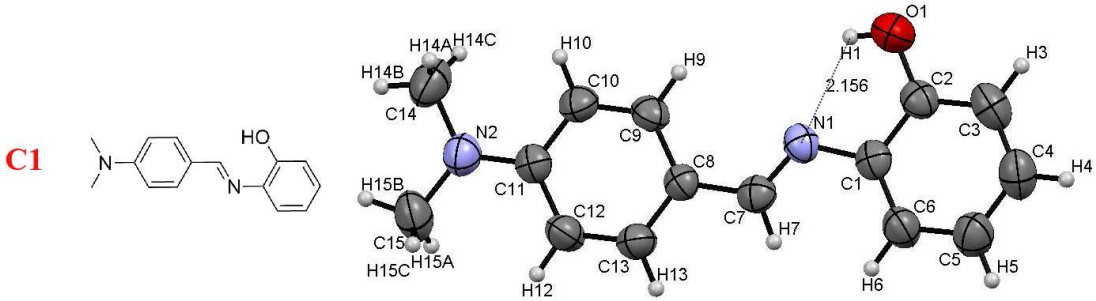

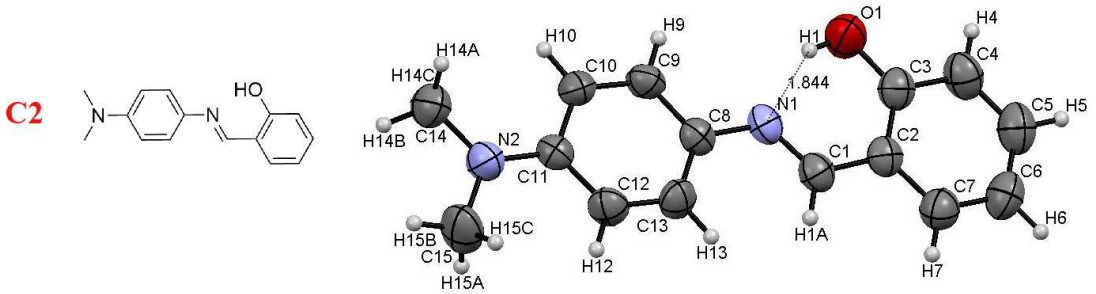

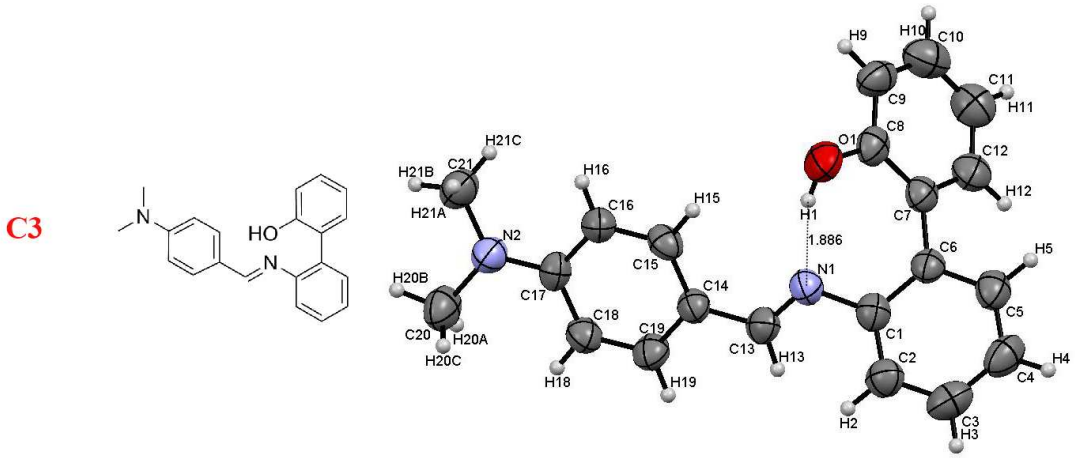

Figure 1 ORTEP drawing of **C1**, **C2** and **C3** with 30% possibility of thermal ellipsoids

Hence, the formation of irregular number-membered ring transition states in **C1** and **C3** could be harder than that of six number-membered one in **C2**. Furthermore, the stability of six number-membered ring transition state in **C2** could be greater than that of five- and seven-number-membered ones in **C1** and **C3** respectively. Thus, it is deduced that the energy barriers of five- and seven- number-membered ring transition states in **C1** and **C3** can be much larger than six number-membered one in **C2** respectively. As a consequence, it is more difficult to undergo intramolecular proton transfer through five- and seven- number-membered ring of transition states in **C1** and **C3** respectively.

X-ray single crystal diffraction analysis also demonstrates that C=N double band in **C2** shows the greater coplanarity than **C1** and **C3** respectively, which means the presence of the greater steric hindrances between the adjacent hydroxy and imino groups in **C1** and **C3**. It is found that the dihedral angle of ∠C8-N1-C1-C2 in **C2** is 0.65˚, while the dihedral angle of ∠C1-N1-C7-C8 in **C1** is 1.59˚, and the dihedral angle of ∠C1-N1-C13-C14 in **C3** increases to 2.34˚.

2.2. Intramolecular hydrogen bond based on analysis of ^{1}H-NMR spectra

It is known that hydrogen bond leads to a downshift of ^{1}H-NMR peak of a bridge hydrogen

atom due to deshielding effect.[20] ^{1}H-NMR chemical shifts of phenolic hydroxy group in the targets move to the lower magnetic field comparing to those in the references (see **Figures S1** in ***Supplementary materials***, such as **C1**, 8.659 ppm, **C7**, 8.187 ppm). In addition, ^{1}H-NMR chemical shifts of imino groups in the references are located at the higher magnetic field comparing to those in target molecules (such as **C1**, 8.489 ppm and **C4**, 8.257 ppm, **Figures S1**). Hence, ^{1}H-NMR spectra further suggest that there is presence of intramolecular hydrogen bond in the target molecules.

^{1}H-NMR peak of phenolic hydroxy group in **C2** shifts to the lower magnetic field than that of **C1** and **C3** respectively (such as **C1**, 8.659 ppm and **C3**, 10.847 ppm *versus* **C2**, 13.634 ppm, **Figure S1**). Meanwhile, ^{1}H-NMR peak values of imino group in **C1** and **C3** are lower than that of **C2** respectively (such as **C1**, 8.489 ppm and **C3**, 8.402 ppm *versus* **C2**, 8.889 ppm, **Figure S1**). Hence, ^{1}H-NMR spectra further suggest that intramolecular hydrogen bond between adjacent hydroxy and imino groups in **C1** and **C3** is much weaker than that in **C2**.

2.3. Intramolecular hydrogen bond effect on ultraviolet/visible spectra

The ultraviolet/visible spectra of the target and reference molecules were studied in various organic solvents. The typical UV/visible spectra of target molecules **C1**, **C2** and **C3** in 1,4-dioxane and DMF are shown in **Figure 2**. The representative UV/visible spectral parameters are presented in **Table 1**.

It is found that the target dyes **C1**, **C2** and **C3** show similar ultraviolet/visible spectral shapes to the methylated references, which exhibit long-wavelength absorption bands in 350~500 nm region (also see **Figure S2** & **Table S1**). In contrast, the reduced references are absence of such long-wavelength absorption bands (**Figure S2**). The results suggest that there is presence of

internal charge transfer in ground states of the target dyes and the methylated references, while the reduced references are deficient in intramolecular charge transfer due to lack of electron-withdrawing imino group.

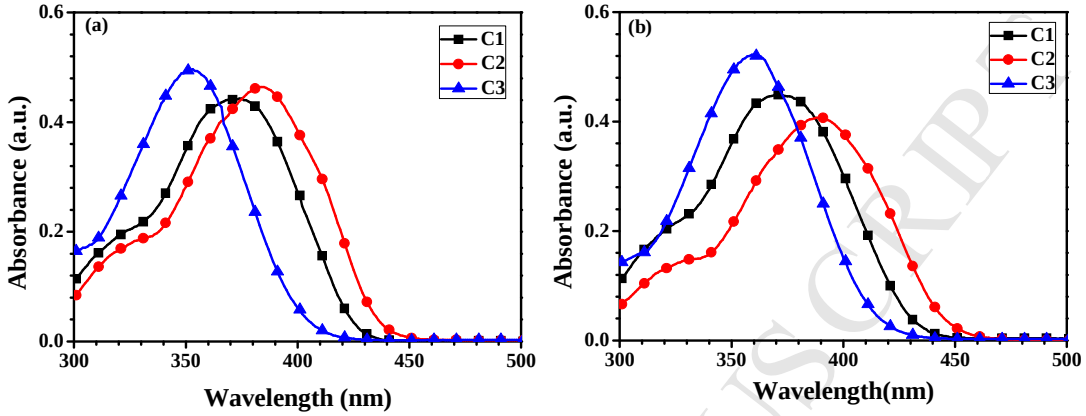

Figure 2 UV/visible absorption spectra of **C1**, **C2** and **C3** in 1,4-dioxane(a) and in DMF (b), the concentration is 2×10^{-5} mol/L

Table 1 The absorption and emission spectral parameters of **C1**, **C2** and **C3** in various solvents, $\lambda_{a,max}$: the absorption maximum (nm), $\lambda_{f,max}$: the emission maximum (nm), ε_{max}: the maximal molar extinction coefficient ($10^5 \bullet cm^{-1} \bullet mol^{-1} \bullet L$), Φ: the fluorescence quantum yield

Solvents	C1				C2				C3			
	$\lambda_{a,max}$	$\lambda_{f,max}$	Φ	ε_{max}	$\lambda_{a,max}$	$\lambda_{f,max}$	Φ	ε_{max}	$\lambda_{a,max}$	$\lambda_{f,max}$	Φ	ε_{max}
Benzene	379	433	0.0671	0.333	388	433, 527	0.0490	0.286	372	426	0.0835	0.348
1,4-dioxane	372	411	0.0321	0.210	384	406, 531	0.0971	0.176	373	401	0.0560	0.259
THF	375	424	0.0772	0.254	386	434, 531	0.0324	0.247	377	434	0.0528	0.356
EtOAc	373	413	0.0191	0.288	379	435, 526	0.0589	0.106	373	434	0.0484	0.262
CH_2Cl_2	380	411	0.0339	0.295	379	430, 535	0.0873	0.221	378	414	0.0457	0.208
$CHCl_3$	379	413	0.0328	0.356	387	433, 533	0.0739	0.190	375	418	0.0367	0.189
MeCN	374	422	0.0668	0.318	384	436, 542	0.0668	0.240	378	434	0.0189	0.281
DMSO	370	411	0.0797	0.197	392	433, 548	0.0913	0.171	381	432	0.0366	0.227
DMF	372	413	0.0647	0.212	389	426, 535	0.0847	0.217	360	433	0.0704	0.243

It is further observed that the maximal absorption wavelengths of targets **C1**, **C2** and **C3** are a little red-shifted with respect to those of the methylated references (**Figure S2**). This means that intramolecular hydrogen bond in the target molecules enhances extent of intramolecular charge

transfer in ground states. In addition, the absorption maxima of **C1**, **C2** and **C3** are basically in the order as **C2**>**C3**>**C1** in various solvents, reflecting the consequence of intramolecular hydrogen bond strength.

2.4. Steady fluorescence emission spectra of the target dyes

Presence of intramolecular hydrogen bond effect in ground state of the target molecules means a large possibility to undergo ESIPT.[21] In order to get the direct experimental evidence of internal proton transfer in excited state, fluorescence emission spectra of the target dyes and the reference molecules were investigated in various organic solvents. The representative fluorescence spectra of **C1**, **C2** and **C3** in 1,4-dioxane and DMF are given in **Figure 3**. The typical fluorescence spectral parameters are depicted in **Table 1**.

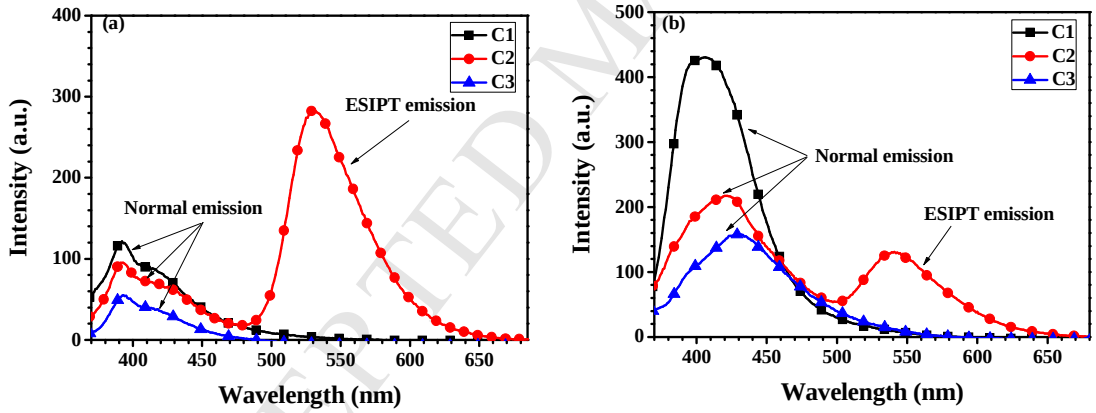

Figure 3 Steady emission spectra of **C1**, **C2** and **C3** in 1,4-dioxane(a) and in DMF (b), the concentration is 5×10^{-6} mol/L for the emission spectra, Excitation at 350 nm

It is observed that the targets **C1** and **C3** show single emission band in various solvents, which is almost identical to the corresponding reference molecules such as **C4** and **C6** (**Figure S3**). The emission maxima of **C1** and **C3** and the corresponding methylated references are located around 430 nm (**Table S1**), which are red-shifted to those of the reduced references such as **C7** and **C9** due to more intensive internal charge transfer (**Figure S3**).

It is noticed that **C2** exhibits dual-emission bands in various solvents. While in contrast, the reference molecules **C5** and **C8** display single emission band (**Figure S3**). It is shown that the emission maxima of the first emission band of **C1** is close to the maximal emission wavelengths of the reference molecules as well as the other target molecules (**Table S1**).

It is found that the maximal emission wavelengths of **C2** are much red-shifted with respect to those of the first emission bands (426 nm *versus* 535 nm in DMF). As a consequence, the fluorescence emission of the first emission band of **C2** possess the normal Stokes-shift (~37 nm in DMF), while the second fluorescence band of **C2** is characterized with the large Stokes-shift (~146 nm in DMF). Therefore, the results show that the fluorescence emission of **C1** and **C3** is yielded by the excited normal enol decay, which is effectively the same as $S_0 \rightarrow S_1$ enol absorption spectral feature. However, the second emission band of **C2** is produced by the decay of the excited keto.[22] The results demonstrate that **C1** and **C3** cannot process internal proton transfer in excited state through five- and seven- number-membered ring transition states, while **C2** undergoes ESIPT through a six- number-membered ring transition state. This could be ascribed to the stronger internal hydrogen bond in **C2** comparing to that in **C1** and **C3**.

It is further found that the target dyes show similar fluorescence spectral properties in solid state or in polymer matrix as those in organic solvents respectively in **Figure S4**. **C2** exhibits strong ESIPT emission, while the solids **C1** and **C3** show only normal enol emission. The results further demonstrate that it is more easily to undergo ESIPT through a six- number-membered ring transition state than irregular number-membered ring ones in various environments.

It is necessary to point out that although the reported benzimidazole-phenol derivatives can undergo ESIPT via a six number-membered ring transition state, the most of emission maxima of

keto tautomers are below 500 nm in various states [23-25], and only a few efforts have been made to achieve above 500 nm keto emission successfully [26, 27]. It is noticed that phenolic hydroxy group in benzimidazole-phenol derivatives normally shows a higher magnetic field ^{1}H-NMR chemical shift (~ 11 ppm), and thus a weaker hydrogen bond could be a detriment to its ESIPT process, leading to a hyperchromic shift of keto emission maxima due to the influence of competitive normal (π, π^*) decay. While free C=N bond in **C2** could offer a greater diversity than restricted C=N bond in benzimidazole-phenol derivatives, which increases intramolecular hydrogen bond strength between O-H and C=N groups because it is not limited toward a specific direction. As a consequence, a six number-ring transition state could be yielded and its potential energy barrier of E^* to K^* could be diminished, resulting in increasing ESIPT maximum.

2.5. Time-resolved fluorescence emission spectra

Phototautomers enol and keto forms of **C2** can be well distinguished from each other in the time-resolved fluorescence spectra obtained by the decay kinetics basing on the dependence of emission wavelength. **Figure 4** shows that the maximal transient tautomer enol emissive peak of **C2** in DMF is yielded at 1.5×10^{-11} s, while the intensity decreases with the decay time course. Meanwhile, the maximal transient keto peak is found at 3.5×10^{-11} s decay time range. After then, the both of transient products show the decrease emission with decay. Thus, time-resolved fluorescence emission profiles of **C2** further demonstrate intramolecular proton transfer in excited state. In contrast, there are only transient tautomer enol emissive peaks for **C1** and **C3**, suggesting the absence of intramolecular proton transfer in excited states of **C1** and **C3** (**Figure S5**).

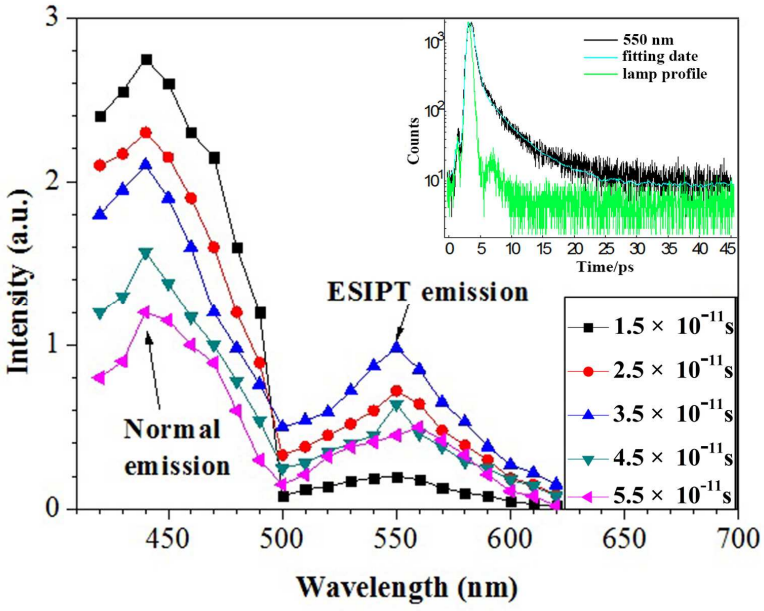

Figure 4 Time-resolved fluorescence spectra of **C2** in DMF, the concentration is 5×10^{-5} mol/L

It is observed that the fluorescence lifetime of the first emission band of **C2** is close to that of the other targets **C1** and **C3** respectively (such as in 1,4-dioxane, **C1**, 3.71×10^{-11} s at 420 nm, **C2**, 3.62×10^{-11} s at 416 nm, **C3**, 3.86×10^{-11} s at 413 nm). The methylated references also yield the similar fluorescence lifetimes to those of the first emission bands of **C2** (such as in 1,4-dioxane, **C4**, 3.53×10^{-11} s at 413 nm). The results further demonstrate that the excited enol form accounts for the first emission band of **C2** in various solvents. It is further found that the second emission band of **C2** show much shorter fluorescence lifetime in various solvents (such as in 1,4-dioxane, 2.11×10^{-12} s at 550 nm), indicating that the excited keto form could have a more competitive radiative transition than the excited enol form.

The radiative and non-radiative transition rates in excited state of a dye can be calculated by the following equations:

$$k_r=\Phi_f/\tau_f \qquad (1)$$

$$k_{nr}=(1-\Phi_f)/\tau_f \qquad (2)$$

wherein Φ_f is fluorescence quantum yield of a dye and τ_f shows lifetime determined at the maximal emission wavelength of fluorescence band of a dye.

Since the fluorescence emission of **C2** includes the enol fluorescence band and the keto fluorescence band, the fluorescence quantum yield of **C2** can be regarded as the sum of the normal fluorescence quantum yield and ESIPT fluorescence quantum yield, as shown in the following equation:

$$\Phi_{f\,(sum)} = \Phi_{f\,(enol)} + \Phi_{f\,(keto)} \qquad (3)$$

Because the absorption of **C2** is assigned to tautomer enol to enol*, the ratio of the integrated area of the normal emission band or the ESIPT emission band to that of the total emission represents the percent of the normal emission band or the ESIPT emission band to the total fluorescence emission respectively. Consequently, the normal fluorescence quantum yield and ESIPT fluorescence quantum yield of **C2** can be calculated respectively. Accordingly, the radiative and non-radiative transition rates of the tautomers enol decay and keto decay in excited state of **C2** can be calculated.

The radiative and non-radiatibe transition rates of **C1**, **C2** and **C3** are give in **Table 2**. The data suggest that ESIPT emission band of **C2** exhibit larger radiative transition rates than the normal emission band in various organic solvents (such as in DMF, **C2**, $k_{r(keto)}$, 3.86×10^{10} s^{-1}, $k_{r(enol)}$, 3.65×10^{9} s^{-1}), suggesting that the decay of excited keto form of **C2** is strong competitive in excited state. It is also found that the nonradiative transition rates of **C1** and **C3** are lower than those of the normal emission band of **C2**, which indicates that internal proton transfer decrease the transition decay of the excited enol form.

Table 2 Radiative transition rates (s^{-1}) of the tautomers enol and keto decay in excited state of **C1**, **C2** and **C3**

Dyes		Solvents	
		1,4-dioxane	**DMF**
C1	$\Phi_{f\,(enol)}$	0.0321	0.147
	$\tau_{f\,(enol)} \times 10^{-11}$ (s)	3.71	1.65
	$k_{r\,(enol)} \times 10^{10}$ (s^{-1})	0.0865	0.891
	$k_{nr(enol)} \times 10^{11}$ (s^{-1})	0.261	0.517
C2	$\Phi_{f\,(enol)}$	0.0238	0.0500
	$\tau_{f\,(enol)} \times 10^{-11}$ (s)	3.62	1.37
	$k_{r\,(enol)} \times 10^{10}$ (s^{-1})	0.0657	0.365
	$k_{nr\,(enol)} \times 10^{11}$ (s^{-1})	0.270	0.693
	$\Phi_{f\,(keto)}$	0.0733	0.0347
	$\tau_{f(keto)} \times 10^{-12}$ (s)	2.11	0.901
	$k_{r\,(keto)} \times 10^{11}$ (s^{-1})	0.347	0.386
	$k_{nr(keto)} \times 10^{12}$ (s^{-1})	0.439	1.07
C3	$\Phi_{f\,(enol)}$	0.0560	0.0704
	$\tau_{f\,(enol)} \times 10^{-11}$ (s)	3.86	1.76
	$k_{r\,(enol)} \times 10^{10}$ (s^{-1})	0. 145	0.401
	$k_{nr(enol)} \times 10^{11}$ (s^{-1})	0.245	0.528

2.6. Molecular geometry optimization

2.6.1. Geometrical parameters

The theoretical calculation was performed to understand the experimental results. The optimized structures of enol, keto and transition state (TS) forms in excited states of **C1**, **C2** and **C3** are shown in **Figure S6**, and the corresponding structural parameters are listed in **Table 3**. It is shown that TS form of enol-keto phototautomerization in excited state of **C1** cannot be obtained, which means that energy keeps either going up or down all the time during E-K phototautomerization.

As we expected, the distances of H-O in TS of enol-keto tautomerization of these molecules are between those of tautomers in S_0 or S_1 states (such as H-O in S_1 of **C2**, E^*, 0.945 Å, TS, 1.214 Å, K, 1.846 Å, **Table 3**). Furthermore, the distances of O-N in TS forms are smaller than those of E and K forms in S_0 or S_1 states (such as O-N in S_1 of **C2**, E^*, 2.822Å, TS, 2.395Å, K, 2.668 Å,

indicating that TS forms of these molecules possess the more intensive internal hydrogen bond than enol and keto forms.

Table 3 The most important distances association with ESIPT calcualted at HF level for ground state and at CIS level for excited state to **C1**, **C2** and **C3** respectively

Structural parameters		Ground state			Excited state		
Distances (Å)		E	TS	K	E^*	TS^*	K^*
C1	R_{O-H}	0.947	1.374	1.885	0.950		2.045
	R_{N-H}	2.156	1.158	1.018	2.131		0.999
	R_{O-N}	2.693	2.342	2.539	2.666		2.576
C2	R_{O-H}	0.954	1.273	1.868	0.945	1.214	1.846
	R_{N-H}	1.886	1.184	1.005	2.053	1.240	1.008
	R_{O-N}	2.711	2.385	2.656	2.822	2.395	2.668
C3	R_{O-H}	0.949			0.948	1.311	1.625
	R_{N-H}	3.919			2.990	1.323	1.015
	R_{O-N}	4.264			3.848	2.417	2.597

As compared with **C1** and **C3**, the smallest N-H in ground and excited states of **C2** suggests that there is the strongest hydrogen bond in **C2** as well as the shortest tunnel of intramoleular proton transfer, which is thus favorable for ESIPT to **C2**. As shown in **Table 4**, the important dihedral angles of ∠C-H-O-N as well as ∠C-C-N-C in *o*-hydroxy-phenyl-imino part of the target dyes are acquired. As compared with **C1** and **C3**, the greatest coplanar excited TS form of **C2** shows that there is the largest possibility to undergo enol-keto phototautomerization in excited state of **C2** (such as $\angle C_1$-O_1-H_1-N_1 in **C2**, 0.307 ˚, $\angle C_1$-O_1-H_1-N_1 in **C3**, 32.212 ˚). In contrast, TS form in the excited state of **C3** shows the poor coplanarity, which means that it is hard for **C3** to process intramolecular proton transfer in excited state.

Table 4 The most important dihedral angle calcuted at HF level for ground state and at CIS level for excited state to **C1**, **C2** and **C3** respectively

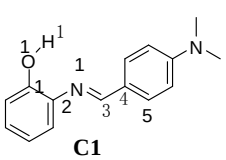

C1

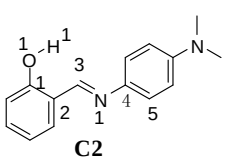

C2

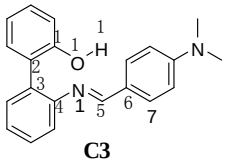

C3

Structural Parameters		Ground state			Excited state		
	Angle (°)	E	TS	K	E^*	TS^*	K^*
C1	∠C_1-O_1-H_1-N_1	-5.215	0.012	0.001	0.082		0.006
	∠N_1-C_3-C_4-C_5	-5.051	-0.060	-0.003	-5.547		0.001
	∠C_1-C_2-N_1-C_3	29.812	-0.022	0.002	0.710		0.001
C2	∠C_1-O_1-H_1-N_1	-0.019	0.830	2.780	30.299	0.307	0.103
	∠C_3-N_1-C_4-C_5	41.933	35.846	35.188	0.361	0.345	0.505
	∠C_1-C_2-N_1-C_3	0.800	-0.393	-0.101	-7.100	0.046	-0.067
C3	∠C_1-O_1-H_1-N_1	-44.305			20.325	32.212	49.303
	∠C_3-C_4-N_1-C_5	-60.857			14.692	6.621	7.584
	∠N_1-C_5-C_6-C_7	0.112			5.407	2.899	1.912

2.6.2. Energy barriers of enol-ketotautomerization of in S_0 and S_1 states

Since enol-keto tautomerization is a typical organic chemical reaction, the potential energy curves (PEC) of intramolecular proton transfer of the target molecules are drawn considerable attentions. Hence, the PEC for ESIPT of the studied dyes was calculated by specifying a reaction coordinate of the distance from O atom to H atom. **Figure 5** and **Figure S7** show the plots of the potential energy curves in S_0 and S_1 states of the molecules **C1**, **C2** and **C3** respectively.

Firstly, the instability of the K form in ground state of **C3** indicates the inviability of ground state intramolecular proton transfer. As shown in **Figure 5**, the energy barrier of E-K in excited state of **C3** is too large (~50 kcal/mol) and the energy of the keto form is much higher than that of enol form, suggesting the great impossibility of intramolecular proton transfer in excited state of **C3**.

It is further found that there is absence of TS form in excited state of **C1** and K form is more unstable in excited state in **C1**. The energy of E-K in excited state of **C1** keeps increasing, which shows ESIPT ($E \rightarrow E^* \rightarrow K^* \rightarrow K \rightarrow E$) cannot occur to **C1**. In contrast, the energy of K form in

excited state of **C2** is much lower than that of enol form, suggesting K form is more stable in excited state of **C2**. Furthermore, a quite small energy barrier of E-K in excited state of **C2** can be easily overcome (~5 kcal/mol). Hence, intramolecular proton transfer in excited state of **C2** is much more possible. It is interesting that **C2** has a smaller reversible energy barrier (K→E) than **C1** and **C3** in ground state (see **Figure S7**), which further suggests that **C2** possesses a greater ability to achieve ESIPT four-level cycle process.

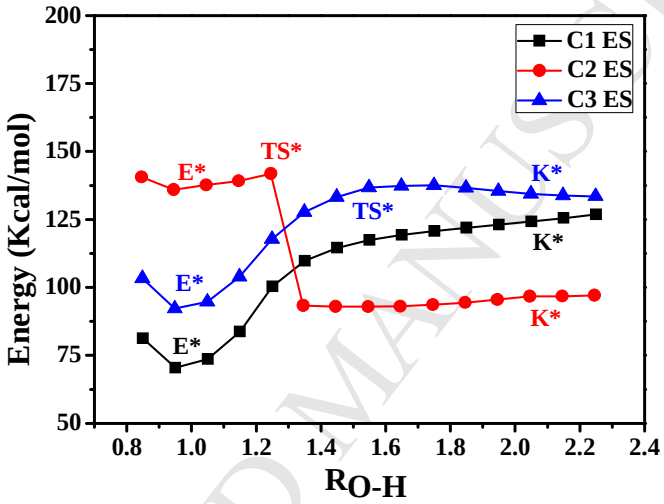

Figure 5 Proton transfer reaction potential energy curves relaxed along the O-H distance at the first excited single state for **C1**, **C2** and **C3**

2.6.3. Frontier orbitals, Mulliken atomic charge and dipole moment

Since ESIPT occurs in excited state, we particularly concentrate on frontier orbitals of the excited state enol tautomers. It is noticed that the electron cloud in mainly distributed at the N,N-dimethyl-phenyl part in HOMO of excited **C2** (**Figure S8**), while it is mainly located at phenyl-imino part in LUMO. This means that phenyl-imino part could be greatly active in the excited LUMO of enol form of **C2**

In contrast, there is presence of major electron cloud density distribution in phenyl-imino part in HOMOs of excited enol forms of **C1** and **C3**, while it is mainly distributed in

N,N-dimethyl-phenyl part in LUMOs. The deficiency of electron cloud density distribution in phenyl-imino part in LUMOs of excited enol forms of **C1** and **C3** suggests that phenyl-imino part could be inactive in excited LUMO of enol forms of **C1** and **C3**. Hence, the frontier orbital nature of the excited enol tautomers shows that **C2** has a more possibility to process internal proton transfer in excited state than **C1** and **C3**.

Table 5 Mulliken net atomic charges of the key atoms of the molecules **C1**, **C2** and **C3**

Mulliken Charge (e)		**E**			
		C	O	H	N
Ground State	**C1**	0.381	-0.668	0.369	-0.636
	C2	0.428	-0.683	0.402	-0.682
	C3	0.386	-0.674	0.355	-0.579
Excited State	**C1**	0.342	-0.671	0.373	-0.793
	C2	0.447	-0.653	0.387	-0.782
	C3	0.384	-0.698	0.378	-0.796

It is further found that as E of **C2** is excited to E^*, oxygen atom of phenolic group shows a decrease of negative charge, and hydrogen atom of phenolic group exhibits a decrease of positive charge as well (**Table 5**, -0.683 e to -0.653 e for O atom, 0.402 e to 0.387 e for H atom). While, an opposite tendency is found during E to E^* transition of **C1** and **C3** (such as to **C3**, -0.674 e to -0.698 e for O atom, 0.355 e to 0.378 e for H atom). The results indicate that phenolic group in **C2** is more loose and active than that of **C1** and **C3**. As a result, the proton in phenolic group of **C2** is more reactive accordingly.

It is noticed that the tautomers of **C2** show a quite lower dipole momenet change from the ground state to the excited state than those of **C1** and **C3** (**Table 6**, such as enol form of **C2**, 2.925 D to 3.742 D; such as enol form of **C3**, 3.052 D to 10.596 D), which indicates that it requires a smaller energy to undergo such diople moment change for **C2** as compared with **C1** and **C3**. The results are consistent with the above energy barrier calculation.

Table 6 Dipole moment of each tautomer calculated at HF level for ground state and at CIS level for excited state to **C1**, **C2** and **C3** respectively

Dipole moment (D)	Ground state			Excited state		
	μ_E	μ_{TS}	μ_K	μ_E	μ_{TS}	μ_K
C1	4.480	9.551	11.631	8.573		12.607
C2	2.925	4.565	4.971	3.742	4.713	5.576
C3	3.052			10.596	17.429	21.172

3. Conclusions

To be closing, this study aims to deal with a long-staying chemical question why it is hard to undergo internal proton transfer in excited state through irregular number-membered ring transition states. For this purpose, a range of organic dyes carrying similar chemical structures that could undergo intramolecular proton transfer in excited states via different number-membered ring transition states respectively. The different strength of internal hydrogen bond in the studied dyes is demonstrated by X-ray single crystal diffraction, NMR spectra as well as UV/visible spectra. The intramolecular proton transfer in excited state of the studied dyes is strongly competitive through a six number-membered ring transition state, while no experimental evidence support the occurrence of ESIPT via five- and seven- number-membered ring transition states of the studied dyes respectively. The optimized geometric parameters association with internal proton transfer such as the distance between two atoms and dihedral angles of proton transfer segments suggest that it is more difficult to undergo ESIPT via irregular five- and seven- number-membered ring transition states of the studied dyes. The other calculated results including energy barriers of enol-keto phototautomerization of and frontier orbital properties in S_1 states of the studied dyes as well as Mulliken atomic charge support such conclusions as well. Therefore, in order to achieve intramolecular proton transfer in excited state through irregular number-membered ring transition

states, these disadvantages much be minimized. The results presented in this study would be greatly beneficial for the synthesis of new organic chromophores undergoing ESIPT via different number-membered ring transition states.

4. Experimental

4.1. Reagents and characterization

The organic solvents were supplied by Aldrich Corporation, which were further processed by standard laboratory methods.[28] The target molecules were synthesized in our own laboratory (**Scheme S1, *Supplementary materials***), in which **C3**, **C6** and **C9** were firstly reported in this study.

Nuclear magnetic resonance (NMR) spectra of the samples were determined by Bruker 400 MHz, 500 MHz and 600 MHz apparatus in standard NMR tubes at room temperature. The chemical shifts of hydrogen and carbon atoms in NMR spectra were identified by using tetramethylsilane (TMS) as an internal reference. Nicolet 550II Fourier transform infrared spectrometer was employed to measure IR spectra of the samples (KBr pellet method). A CE440 elemental analysis meter from Exeter Analytical Inc was used to conduct elemental analysis of the samples. High resolution mass spectra (HRMS) electro spray ionization (ESI) was conducted by a UPLC-Q-ToF MS spectrometer. A Beijing Fukai melting point apparatus was employed to determine the melting points of the samples.

Slow volatilization of organic solvents in NMR tubes to obtain single crystals of the samples. A suitable single crystal was put inside a glass fiber capillary to determine molecular structure by X-ray diffraction, which was analyzed by the direct methods and refined by full-matrix least squares on F^2. XRD data were acquired by a Bruker-AXS CCD area detector equipped with

diffractometer with Mo K_a (λ = 0.71073 Å) at 298 K. All the hydrogen atoms were identified in the calculated positions respectively and all the non-hydrogen atoms were analyzed by anisotropic temperature factors.

4.2. UV/visible absorption and fluorescence emission spectral determination

Spectral grade organic solvents were utilized for spectroscopic measurement of the samples. The ultraviolet/visible absorption spectra of the samples were recorded by a TU1901 spectrophotometer from Beijing PUXI General Equipment Limited Corporation. The steady fluorescence emission spectra were determined by Shimadzu RF-531PC spectrofluorophotonmeter. The fluorescence quantum yields of the samples were measured by using Quinine sulfate in 0.5 mol/L H_2SO_4 (Φ, 0.546) as the reference[29] by the equation (4)[30]:

$$\Phi_f = \Phi_f^0 \frac{n_0^2 A^0 \int I_f(\lambda_f)\mathrm{d}\lambda_f}{n^2 A \int I_f^0(\lambda_f)\mathrm{d}\lambda_f} \qquad (4)$$

wherein n_0 and n represent the refractive indices of the solvents for the reference and sample respectively, A^0 and A are the absorption intensities at excitation wavelength, Φ_f and Φ_f^0 show the fluorescence quantum yields of the sample and reference, and the integrals are the areas of the fluorescence emission bands for the reference and sample respectively. The absorption of the sample at excited wavelength is guaranteed below 0.1 to minimize experimental errors. The sample in organic solvents was deaerated by bubbling argon for half of an hour before the measurement of fluorescence spectra.

The fluorescence lifetimes of the samples were measured by a laser system. The pump laser pulses were emitted by the amplified frequency doubling directly. Time-dependent laser detection was obtained through a spectrograph using a connected intensified double photodiode array. The pulses were focused onto a sample cuvette containing 100 μm thick fused-silica window and a 250

pm optical path length. The transient spectra were recorded by a ultrafast white-light continuum.

4.3. Geometry optimization computation

Geometry computation of the samples was by 6-31G** basis set in Gaussian 09 program package. The organic solvents were used as the media in theoretical computation. Geometry optimization of enol and keto of phototautomers in ground states (S_0) was conducted by B3LYP method based on density functional theory (DFT) and HF (Hartree-Fock) level respectively,[31] while geometries in the first singlet excited states (S_1) of the molecules was optimized by CIS method (single-excitation configuration interaction). The energies of optimized geometries of S_0 and S_1 states were computed by DFT and TD-DFT (time-dependence DFT) method respectively such as DFT//DFT and DFT//HF (for S_0) and TDDFT//CIS (for S_1).[32]

4.4. Synthesis of the target dyes

The synthesis routes of the target and reference dyes are shown in **Scheme 1**. The preparation of precursors 2'-hydroxybiphenyl-2-amine and 2'-methoxybiphenyl-2-amine was performed by condensation of 2-hydroxyphenylboronic acid or 2-methoxybenzeneboronic acid and 2-bromo aniline with over 80% isolated yields. It is noticed that quite few studies involving free aryl amines Suzuki coupling reactions have ever been reported.

The synthesis and characterization of the studied molecules are shown in ***Supplementary materials***.

Acknowledgements

The authors greatly appreciate Chongqing Natural Science Foundation CSTC2012jjB50007 and CSTC2010BB0216.H. Li is grateful to the Postdoctoral Science Foundation of China for

financial supporting (Grant No. 22012T50762 &2011M501388). This work was also supported by the Graduate Student Innovation Foundation of Chongqing University (CDJX11131146).

Supplementary materials

The synthesis and characterization of the major products including NMR data, IR data, high-resolution MS data as well as elementary analysis of **C1**~**C9** are included in ***Supplementary materials***. The absorption spectra and steady and transient fluorescence emission spectra of the studied dyes in various media are also provided in ***Supplementary materials***. The optimized geometries of enol, TS and keto forms in excited state of the target dyes, the spectral parameters of the dyes in various solutions and the crystallographic data are further contained in the ***Supplementary materials***. The document is available free of charge from website of this journal.

The supplementary crystallographic data for this study can be found in file numbered by CCDC 1502865-1502867, which are available http://www.ccdc.cam.ac.uk/conts/retrieving.html or from the Cambridge crystallographic data center, 12, Union Road, Cambridge CB2 1EZ, UK; fax: 44-1223-336033.

References and notes

1. Suzuki, N.; Fukazawa, A.; Nagura, K.; Saito, S.; Kitoh-Nishioka, H.; Yokogawa, D.; Irle, S.; Yamaguchi, S. *Angew. Chem. Int. Ed.* **2014**, *53*, 8231-8235.

2. Mutai, T.; Sawatani, H.; Shida, T.; Shono, H.; Araki, K. *J. Org. Chem.* **2013**, *78*, 2482-2489.

3. Kim, J.; Heo, W.; Joo, T. *J. Phys. Chem. B* **2014**, *119(6)*, 2620-2627.

4. Zhang, Z. Q.; Yang, C. T.; Liang, L. J.; Xiao, B.; Lu, X.; Liu, J. H.; Sun, Y. Y.; Marder, T. B.; Fu, Y. *Org. Lett.* **2014**, *16*, 6342-6345.

5. (a) Stasyuk, A. J.; Banasiewicz, M.; Cyrański, M. K.; Gryko, D. T. *J. Org. Chem.* **2012**, *77*,

5552-5558. (b) Gargas, D. J.; Gao, H. W.; Wang, H. T.; Yang, P. D. *Nano Lett.* **2011**, *11*, 3792-3796.

6. (a) Xie, L. J.; Chen, Y. H.; Wu, W. T.; Guo, H. M.; Zhao, J. Z.; Yu, X. R. *Dyes & Pigments* **2012**, *92*, 1361-1369. (b) Cui, G. L.; Lan, Z. G.; Thiel, W. *J. Am. Chem. Soc.* **2012**, *134*, 1662-1672.

7. Zhao, J. Z.; Ji, S. M.; Chen, Y. H.; Guo, H. M.; Yang, P. *Phys. Chem. Chem. Phys.* **2012**, *14(25)*, 8803-8817.

8. Zhang, W.; Yan, Y. L.; Gu, J. M.; Yao, J. N.; Zhao, Y. S. *Angew. Chem. Int. Ed.* **2015**, *54(24)*, 7125-7129.

9. Gong, Y. L.; Lu, Y.; Wang, Z. Q.; Zhang, S. T.; Luo, Z. P.; Li, H. R.; Gao, F. *Tetrahedron Lett.* **2015**, *56*, 236-242.

10. Kim, D.; Kwon, J. E.; Park, S. Y. *Adv. Optical Mater.* **2016**, *4*(5), 790-797.

11. Ciuciu, A. I.; Skonieczny, K.; Koszelewski, D.; Gryko, D. T.; Flamigni, L. *J. Phys. Chem. C*, **2013**, *117*(2), 791-803.

12. (a) Gong, Y. L.; Lu, Y.; Ma, H. Y.; Ding G.; Zhang, S. T.; Luo, Z. P.; Li, H. R.; Gao, F. *Chem. Phys. Lett.* **2015**, *619*, 201-207. (b) Ding G.; Lu, Y.; Gong, Y. L.; Ma, L.; Luo, Z. P.; Zhang, S. T.; Gao, F.; Li, H. R. *Tetrahedron* **2016**, *72*, 3040-3056.

13. Jang, D. J.; Kelley, D. F. *J. Phys. Chem.* **1985**, *89(2)*, 209-211.

14. Bardez, E.; Devol, I.; Larrey, B.; Valeur, B. *J. Phys. Chem. B* **1997**, *101*, 7786-7793.

15. Yu, W. S.; Cheng, C. C.; Cheng, Y. M.; Wu, P. C.; Song, Y. H.; Chi, Y.; Chou, P. T. *J. Am. Chem. Soc.* **2003**, *125*, 10800-100801.

16. Singh, R. B.; Mahanta, S.; Guchhait, N. *Chem. Phys.* **2007**, *331(2)*, 189-199.

17. Guo, Z. Q.; Chen, W. Q.; Duan, X. M. *Dyes & Pigments* **2012**, *92(1)*, 619-625.

18. Zhang, Z.; Hsu, Y. H.; Chen, Y. A.; Chen, C. L.; Lin, T. C.; Shen, J. Y.; Chou, P. T. *Chem. Commun*. **2014**, *50(95)*, 15026-15029.

19. Chen, K. Y.; Cheng, Y. M.; Lai, C. H.; Hsu, C. C.; Ho, M. L.; Lee, G. H.; Chou, P. T. *J. Am. Chem. Soc*. **2007**, *129(15)*, 4534-4535.

20. (a) Casanovas, J.; Namba, A. M.; León, S.; Aquino, G. L.; José da Silva, G. V.; Alemán, C. *J. Org. Chem.* **2001**, *66*, 3775-3782. (b) Wagner, G.; Pardi, A.; Wuethrich, K. *J. Am. Chem. Soc.* **1983**, *105*, 5948-5949.

21. (a) Parada, G. A.; Markle, T. F.; Glover, S. D.; Hammarström, L.; Ott, S.; Zietz, B. *Chem.-A Eur. J*. **2015**, *21*, 6362-6366. (b) Tseng, H. W.; Liu, J. Q.; Chen, Y. A.; Chao, C. M.; Liu, K. M.; Chen, C. L.; Lin, T. C. *J. Phys. Chem. Lett.* **2015**, *6*, 1477-1486.

22. Ushuka, B.; Stupaka, A. *J. Lumin.* **2003**, *105*, 81-87; (b) Doroshenko, A. O.; Posokhov, E. A.; Verezubova, A. A.; Ptyagina, L. M. *J. Phys. Org. Chem*. **2000**, *13*, 253-255.

23. Park, S.; Kwon, O. H.; Kim, S.; Park, S.; Choi, M. G.; Cha, M.; Park, S. Y.; Jang, D. J. *J. Am. Chem. Soc*. **2005**, *127(28)*, 10070-10074.

24. Takagi, K.; Sugihara, K.; Isomura, T. *J. Polym. Sci. Part A: Polym. Chem.* **2009**, *47(18)*, 4822-4829.

25. Shaikh, M.; Dutta Choudhury, S.; Mohanty, J.; Bhasikuttan, A. C.; Nau, W. M.; Pal, H. *Chem.-A Eur. J*. **2009**, *15(45)*, 12362-12370.

26. Padalkar V. S.; Tathe, A.; Gupta, V. D.; Patil, V. S.; Phatangare, K.; Sekar, N. *J. Fluoresce*. **2012**, *22(1)*, 311-322.

27. Sun, W. H.; Li, S. Y.; Hu, R.; Qian, Y.; Wang, S. Q.; Yang, G. Q. *J. Phys. Chem. A* **2009**, *113(20)*, 5888-5895.

28. Perrin, D. D.; Armarego, W. L. F.; Perrin, D. R. Purification of laboratory chemicals; Pergamon: New York, NY, **1966**.

29. (a) Ilies, L.; Sato, Y.; Mitsui, C.; Tsuji. H.; Nakamura, E. *Chem. Asian J.* **2010**, *5*, 1376-1381. (b) Men, G. W.; Chen, C. R.; Zhang, S. T.; Liang, C. S.; Wang, Y.; Deng, M. Y.; Shang, H. X.; Yang. B.; Jiang, S. M. *Dalton T.* **2015**, *44*, 2755-2762.

30. (a) Maus, M.; Reitigg, W.; Bonafoux, D.; Lapouyade, R. *J. Phys. Chem. A* **1999**, *103*, 3388-3401. (b) Lukeman, M.; Veale, D.; Wan, P.; Ranjit, V.; Munasinghe, N.; Corrie, J. E. *Can. J. Chem.* **2004**, *82*, 240-253.

31. (a) Zgiershi, M. Z.; Grabowska, A. *J. Chem. Phys.* **2000**, *112*, 6329-6337. (b) Yi, P.; Liang, Y. H.; Cao, C. Z. *Chem. Phys.* **2005**, *315*, 297-302.

32. (a) Liang, Y. H.; Yi, P. G. *Chem. Phys. Lett.* **2007**,*438*, 173-177. (b) Yang, Z. N.; Yang, S. Y.; Zhang, J. P. *J. Phys. Chem. A* **2007**, *111*, 6354-6360.

ACCEPTED MANUSCRIPT